Earth, Planets and Space

FULL PAPER Open Access

Feasibility study on calculating the Q value of shallow media by using a dense seismic array and a large-volume airgun source

Shen Du, YanXiang Yu* and Liang Xiao

Abstract

The feasibility of using a dense seismic array with an airgun source to study the quality factors of shallow media is verified. Data were obtained from 37 stations in the dense seismic array located in Binchuan, Yunnan Province, China, and the amplitude–distance attenuation method and the coda normalization method were applied to calculate the S-wave quality factors in the area. The amplitude–distance attenuation method yielded Q_S^{-1}=0.0260 ± 0.0103, and the frequency-dependent Q_S^{-1} calculated by the coda normalization method can be expressed by the power law $Q_S^{-1}(f) \cong 0.0554 f^{-0.5643}$. The consistency between the results of these two methods shows that a dense seismic array with an airgun source can be used to study the attenuation characteristics of shallow media. The amplitudes at some points deviate substantially from the fitted curve and thus have a certain influence on the fitting results; hence, we must select high-precision data for the calculation. Given the topography, we speculate that the anomalous stations located on the edge of the Binchuan Basin and in the western hilly area are due to the edge effect of the basin and the weak attenuation of the hilly area and that the anomalous station located in the northern Binchuan depocenter is attributable to local site factors. Compared with the Q_S^{-1} estimated by previous studies, the Q_S^{-1} in the Binchuan area is found to lie between those of the hard soil and sedimentary rock and is similar to the Q_S^{-1} in the North China Basin, corresponding to the shallow velocity structure in this area.

Keywords: Airgun seismic source, Dense array, Q value, Amplitude–distance attenuation, Coda normalization

*Correspondence: yuyx@cea-igp.ac.cn

Institute of Geophysics, China Earthquake Administration, Beijing 100081, China

Graphical Abstract

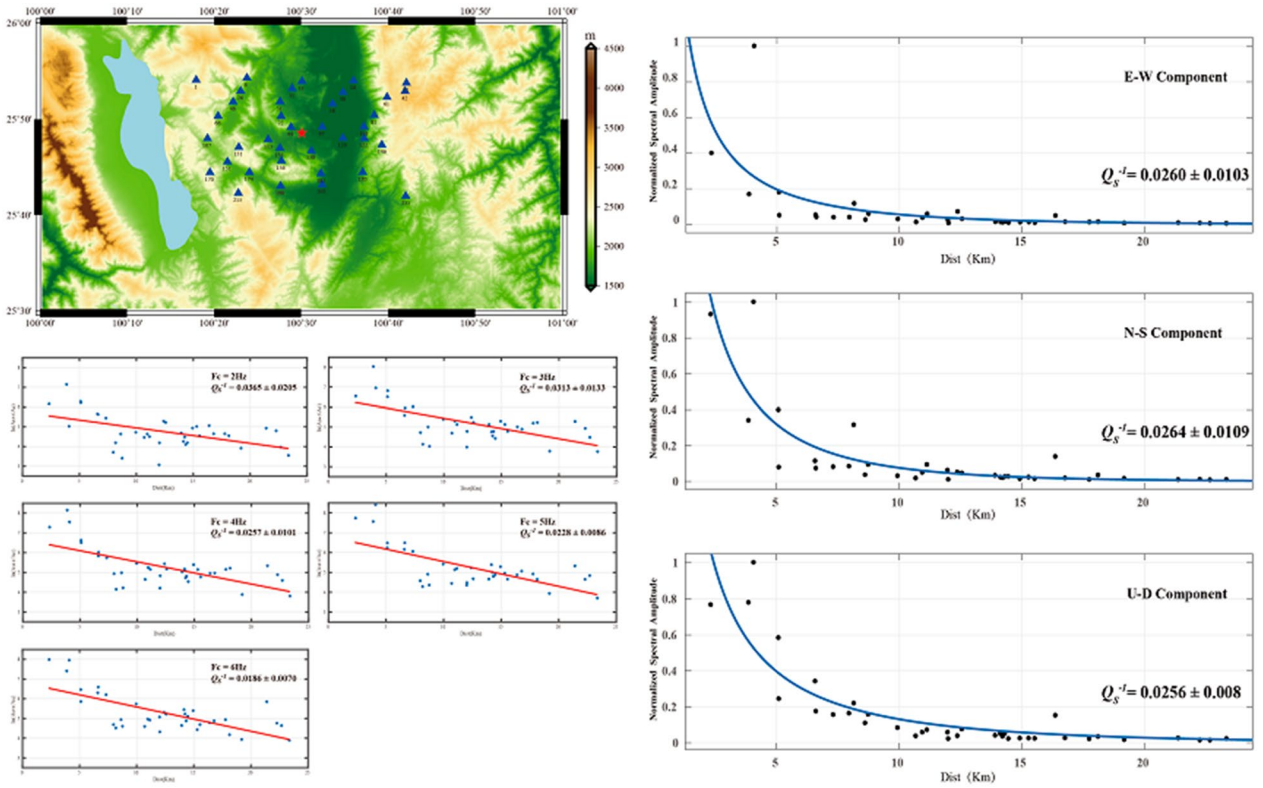

Introduction

The attenuation of seismic waves is an important subject in seismology. The path effect of seismic wave propagation is affected both by geometric attenuation with distance and by the inelastic attenuation of the medium, which is represented by the quality factor Q (Knopoff 1964; Aki 1980a; Castro et al. 1996; Xu et al. 2004; Zhou et al. 2008). The material and physical conditions in the Earth's interior can be inferred from the Q value, one of the fundamental properties of a medium (Anderson and Archambeau 1964; Aki 1980b). The state of rock fractures and changes in fluid activity caused by stress can both affect the Q value, which is more sensitive to changes in underground media than are seismic velocities. Accordingly, seismologists utilize Q values to quantify the Earth's internal media, thermodynamics and structural changes and to monitor the evolution and occurrence of earthquakes (Niu et al. 2008; Su et al. 2015). In engineering seismology, the Q value is a necessary parameter for simulating strong ground motions, predicting ground motions and estimating seismic risk. Hence, the accurate estimation of Q values, especially for shallow media, has an important impact on the peak ground acceleration (PGA) and response spectrum (Sa) of ground motion simulations (Drouet et al. 2005; Wang et al. 2017; Wang 2017).

Limited by the uneven spatiotemporal distribution of natural sources, the accuracy with which variations in the properties of subsurface media can be obtained by natural sources is poor, which mainly affects the estimation of Q values for the Earth's interior, and thus, the characteristics of shallow sedimentary layers cannot be obtained effectively (Wang et al. 2011). In contrast, artificial seismic sources can be operated at any given place and time and can compensate for the shortcomings of natural seismic sources in regional-scale research (Wang et al. 2018). However, because they can cause near-field damage and environmental issues, chemical explosions are highly restricted and cannot be used repeatedly. As an alternative, large-volume airgun sources excited in either natural or man-made lakes was recently proposed to explore inland crustal structures (Chen et al. 2007). The water overlying the airgun source allows the energy to propagate underground, and the waves are diffused outward through the coupling between the water and the solid medium beneath.

Studies have shown that airgun sources are characterized by high signal repeatability, a high energy conversion

efficiency, and abundant seismic phases (Wang et al. 2011). Moreover, multiple excitation signals recorded at the same station can be stacked to enhance the signal-to-noise ratio (SNR) and can be picked at a longer distance than other artificial sources. The signal released by an airgun source includes the pressure pulse produced by the compressed air and the long-period vibration produced by the air-bubble oscillation, which contains rich phase information, especially that of S waves (Caldwell and Dragoset 2000). Therefore, we can use body waves to calculate the Q value.

In previous research on the Q values of body waves, methods such as the hypocenter hypothesis, spectral modeling and spectral ratio were used to separate the attenuation term from the observed waveform to obtain the average Q value of the study area (Su 2009). Solomon and Toksöz (1970) first used the spectral ratio method to compare the spectra of far-field, long-period body waves (epicentral distance > 30°) recorded by two adjacent stations. Since the distance between two such stations is much smaller than their epicentral distances, the source time functions, radiation patterns, site terms and geometric diffusion terms of the signals obtained by these two stations are all approximately the same, and thus, the Q values at different frequencies in the study area can be calculated through the spectral ratio. Aki (1980a) obtained the frequency-dependent S-wave quality factor Q_s in the Kanto area, Japan, by means of the coda normalization method using the ratio of the spectral amplitude of S waves to that of coda waves. Yamaoka et al. (2014) established the amplitude decay relation as a function of distance by utilizing a system of continuously active seismic sources, namely, the Accurately Controlled Routinely Operated Signal System (ACROSS). Based on this method, Su et al. (2015) studied the characteristics of seismic attenuation in the northern Tianshan area using airgun source signals arranged in Hutubi, Xinjiang Province, China, and demonstrated the feasibility of using artificial seismic sources to study the attenuation characteristics of the subsurface.

In this article, we apply data from an airgun source recorded by a dense seismic array in Binchuan, Yunnan Province, China, to calculate the Q_s^{-1} values using the Yamaoka amplitude–distance attenuation relationship and the Aki coda normalization method. The results of these two methods are compared to verify the feasibility and accuracy of using dense seismic array data with an airgun source to quantify the Q values of shallow media.

Method

Amplitude–distance attenuation method

The attenuation of waves with distance is affected not only by the inelasticity and homogeneity of the medium but also by the geometrical spreading of waves. The relationship of the attenuation of body waves with distance (Aki and Richards 1980) can be written as:

$$A = a\frac{1}{x}\exp(-bx), \tag{1}$$

$$b = \frac{\pi f}{Qv}, \tag{2}$$

where x is the distance from the source and a is the intercept term, which is regarded as the source intensity. The term $1/x$ denotes the amplitude decay caused by the geometrical spreading of body waves, while the $\exp(-bx)$ term denotes the attenuation within the medium. b in Eq. 2 is determined by the quality factor Q, frequency f and wave velocity v (Battaglia and Aki 2003). Yamaoka et al. (2014) used the root mean square (RMS) value of the amplitude spectrum in the frequency band to represent the amplitude A at the station. The frequency f corresponding to this amplitude can be calculated by a weighted average:

$$f = \frac{\sum A_i \cdot f_i}{\sum A_i}. \tag{3}$$

Then, the P-wave quality factor Q_p^{-1} and Q_s^{-1} can be obtained by fitting the plot of the RMS amplitudes at seismic stations against the corresponding source distances based on Eqs. 1, 2 and 3 and by substituting the P-wave and S-wave velocities.

Coda normalization method

The second method for measuring Q is the coda normalization method (Aki 1980b), which is based on the idea that coda waves consist of S waves scattered from random heterogeneities in the Earth (Aki 1969; Aki and Chouet 1975; Sato 1977). This principle enables Q_s to be measured from a data set obtained at a single station by normalizing the spectral amplitude of the earthquake source. For local earthquakes, the direct S-wave spectral amplitude As can be expressed as follows after removing the instrumental response and site factor:

$$As(f,r) = S(f,\theta)r^{-1}e^{-\frac{\pi rf}{\beta Q_s(f)}}, \tag{4}$$

where $S(f,\theta)$ is the source spectrum including the radiation pattern, r^{-1} is the geometrical spreading coefficient, and β is the average S-wave velocity. For lapse times greater than twice the direct S-wave traveltime, the spectral amplitude of the coda at lapse time t_c, $Ac(f,t_c)$ is independent of the hypocentral distance r in the regional distance range and is written as:

$$Ac(f,t_c) = S(f)C(f,t_c), \tag{5}$$

where f is the frequency, $S(f)$ is the source spectral amplitude of S waves, and $C(f,t_c)$ is the coda excitation factor. The coda spectral amplitude is proportional to the source spectral amplitude of S waves (Yoshimoto et al. 1993). To normalize the source spectral amplitude of S waves by the spectral amplitude of coda waves, we divide Eq. 4 by Eq. 5:

$$\frac{As(f,r)r}{Ac(f,t_c)} = \frac{S(f,\theta)}{S(f)}C^{-1}(f,t_c)e^{-\frac{\pi rf}{\beta Q_s(f)}}. \tag{6}$$

Since $C(f,t_c)$ is a constant for a fixed t_c irrespective of the hypocenter location, we take the logarithm of Eq. 6 as:

$$\ln\frac{As(f,r)r}{Ac(f,t_c)} = \ln\frac{S(f,\theta)}{S(f)} - \ln C(f,t_c) - \frac{\pi f}{\beta Q_s(f)}r. \tag{7}$$

In order to eliminate the influence of the source radiation pattern, that is to eliminate the first term on the right side of Eq. 7, we take an average of Eq. 7 for a hypocentral distance range $r \pm \Delta r$. Different from the natural source, Jiang (2017) found that the airgun source is isotropic, which radiation pattern is basically circular and radial. The spatial distribution of the signal roughly satisfies the geometric spreading, and the signal from the Binchuan airgun station has no dominant propagation direction (see Additional file 1, Fig. S1). Therefore, we ignore the influence of the airgun source radiation pattern on the source spectrum and finally get the following simple equation:

$$\ln\frac{As(f,r)r}{Ac(f,t_c)} = -\frac{\pi f}{\beta Q_s(f)}r + const(f). \tag{8}$$

When taking the center frequency as f_k, Eq. 8 can be written as:

$$\ln\frac{As(f,r)r}{Ac(f,t_c)} = a - br, \tag{9}$$

where

$$a = const(f_k), b = \frac{\pi f_k}{\beta Q_s(f_k)}. \tag{10}$$

We can estimate $Q_s^{-1}(f_k)$ from a linear regression of $\ln\frac{As(f,r)r}{Ac(f,t_c)}$ versus r by means of the least-squares method:

$$Q_s^{-1}(f_k) = \frac{b\beta}{\pi f_k}. \tag{11}$$

From a set of f_k, we can fit the relationship between the S-wave attenuation and frequency based on the power law $Q_s^{-1}(f) = Q_0^{-1}f^{-\eta}$.

Data and processing

To study the shallow structure of the Binchuan area, the Institute of Geophysics, China Earthquake Administration deployed a dense array of observation stations in the area in 2017. The array was established around the Binchuan Fixed Airgun Signal Transmission Station and covered an area of approximately 40×40 km with an interval of approximately 2 km between stations, which included 380 short-period seismometers. Since this is a feasibility study, we selected 37 stations from this dense array for calculation (Fig. 1). All 37 stations are equipped with the same type of seismometer (EPS), with a flat response from 5 s to 150 Hz and a sampling rate of 200 Hz. These stations are evenly distributed around the source, and the epicentral distance ranges from 2.3 km to 23.4 km.

The signal intensity excited by an airgun is small; the magnitude of each shot is estimated to be only M_L0.9 (Yang et al. 2013), which is greatly affected by noise. However, because an airgun source is repeatedly fired at the same location, it can generate highly repetitive waves, and therefore, the SNR of the signal can be further enhanced through stacking. The dense array in this experiment was operated in three batches, and the number of shots recorded by the seismographs was not uniform (Sun 2019). Hence, we used the maximum number of excitations recorded at each station to perform linear stacking to ensure the quality of stacking. The number of stacks among the 37 stations ranged from 215 to 1073. Figure 2 shows a comparison of a waveform before and after stacking for the East–West (EW) component of station 026, which is the station with the fewest number of shots. The SNR is significantly improved after stacking, indicating that the poststack waveforms can be used for subsequent research.

As a result of the small epicentral distances between the densely arrayed stations and source, the arrival times of the P-wave and S-wave are close, which makes it easy to include the S-wave within the P-wave picking window. Thus, this study uses only S waves for the calculation. To observe the signals clearly, the stacked signals were filtered with a passband of 1–20 Hz, and the arrival times of the P and S waves were picked manually. S waves can be observed from the travel time curve propagating with an apparent velocity of ~ 3.3 km/s (Fig. 3).

Chen et al. (2016) and Zhang et al. (2020) calculated the velocity structure in the Binchuan area based on seismic profile and dense array data. To obtain the average S-wave velocity of the study area, the ray paths of the selected stations were inverted (Fig. 4). The ray path diagrams (Fig. 4a, b) show that the maximum ray penetration depth was approximately 4 km. Therefore, we calculated that the average S-wave velocity over 4 km was approximately 2.87 km/s based on the one-dimensional

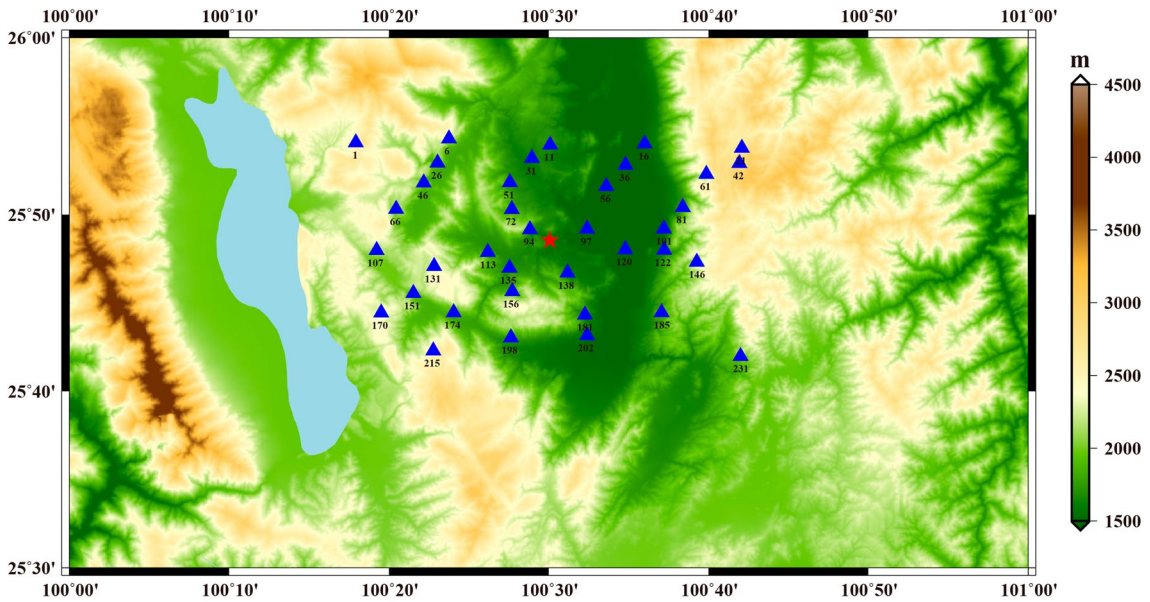

Fig. 1 Locations of the Binchuan Fixed Airgun Signal Transmission Station and the stations. Red star shows the location of airgun signal transmission station, blue triangles denote the location of the 37 stations used in this study

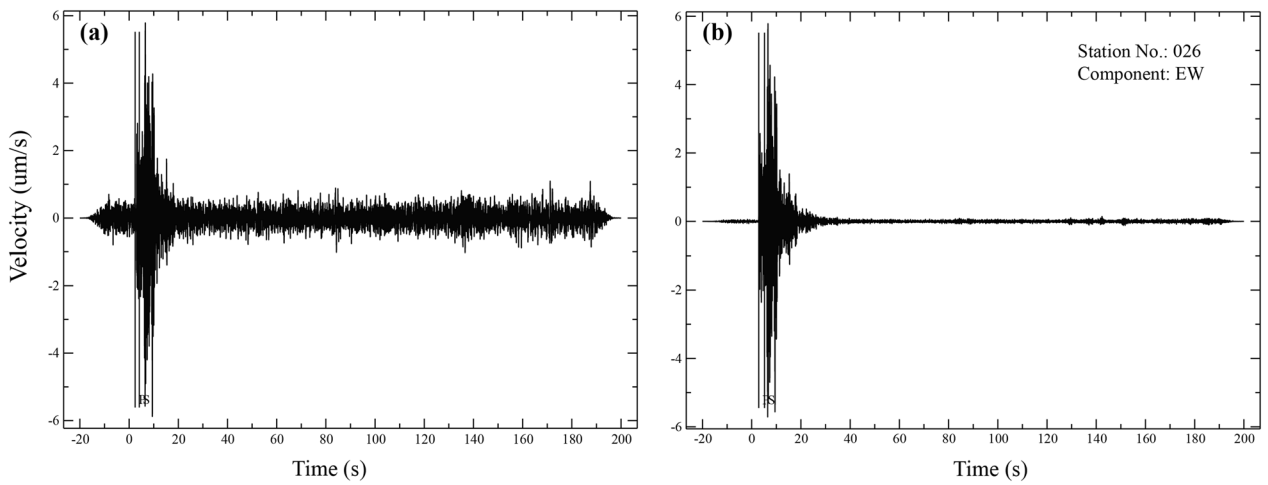

Fig. 2 Comparison of the waveform **a** before stacking and **b** after stacking. It shows the EW component of station 26, with the vertical axis representing velocity in um/s and the horizontal axis indicates time in s

(1-D) velocity model obtained by Chen et al. (2016). Since no significant difference in the amplitudes of EW and North–South (NS) components was observed, we used the EW component records for the S-wave analysis.

Amplitude–distance attenuation method

Spectral analysis was performed on the filtered waveform, which contains the data in an 8-s time window starting from the onset of the S wave, and the frequency–amplitude spectrum of each station was obtained (Fig. 5b). The amplitude spectrum of the airgun signal mainly covers the frequency band of 2 ~ 6 Hz. The amplitude decay relation as a function of distance used by Yamaoka (2014) was used to calculate the RMS amplitude between 2 and 6 Hz as the amplitude of the station. The frequency corresponding to the amplitude is an intermediate frequency, which is calculated by Eq. 3. Combining Eqs. 1 and 2, the attenuation relationship of the amplitude can be fit against the source distance, where v denotes 2.87 km/s. The S-wave

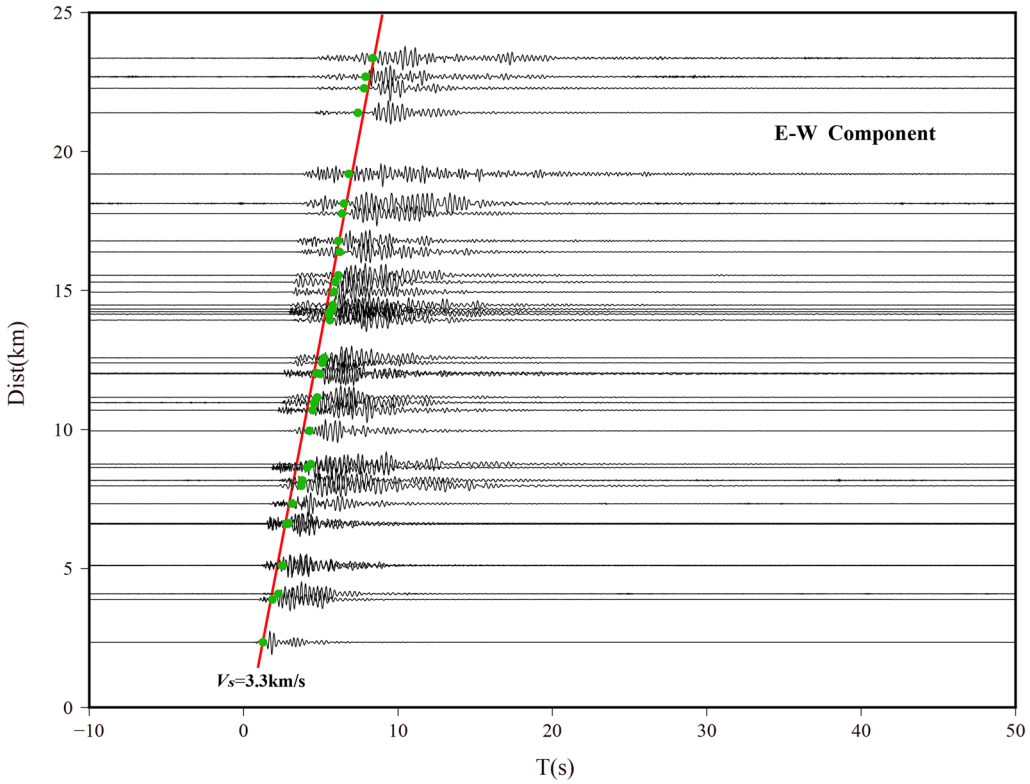

Fig. 3 Travel time curve of S waves. The epicentral distance from the shot point is labeled on the left. The green dots indicate the picked onset of S waves manually, and the slope of red line is 3.3 km/s. The amplitudes at all stations are reduced by a factor of 0.5

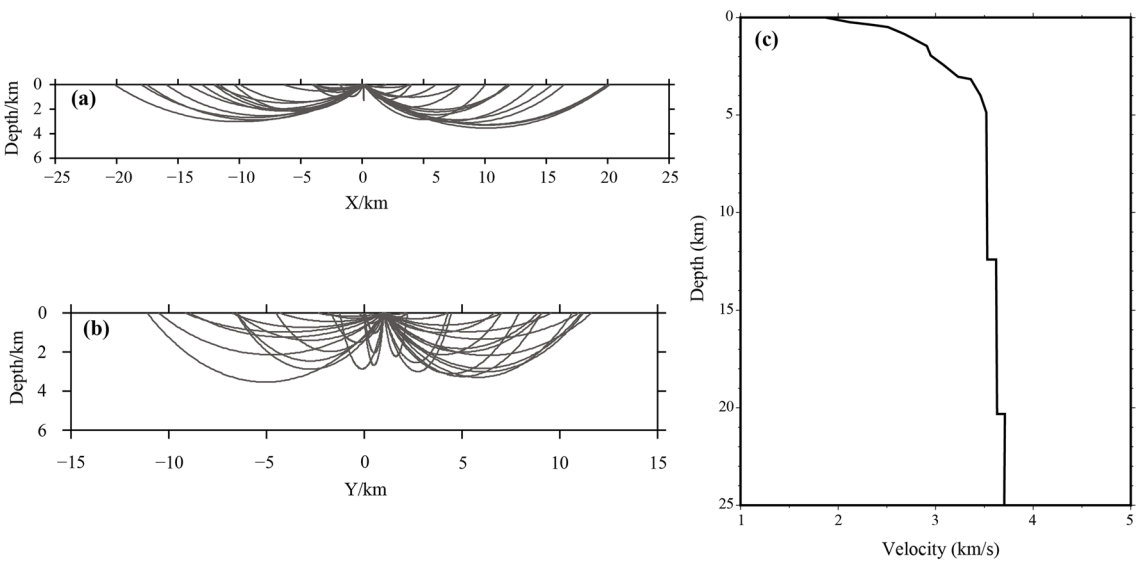

Fig. 4 The ray path and the 1-D velocity model. X in **a** represents the east–west direction, and Y in **b** indicates the north–south direction. **c** is the 1-D S-wave velocity model in the Binchuan area proposed by Chen et al. (2016)

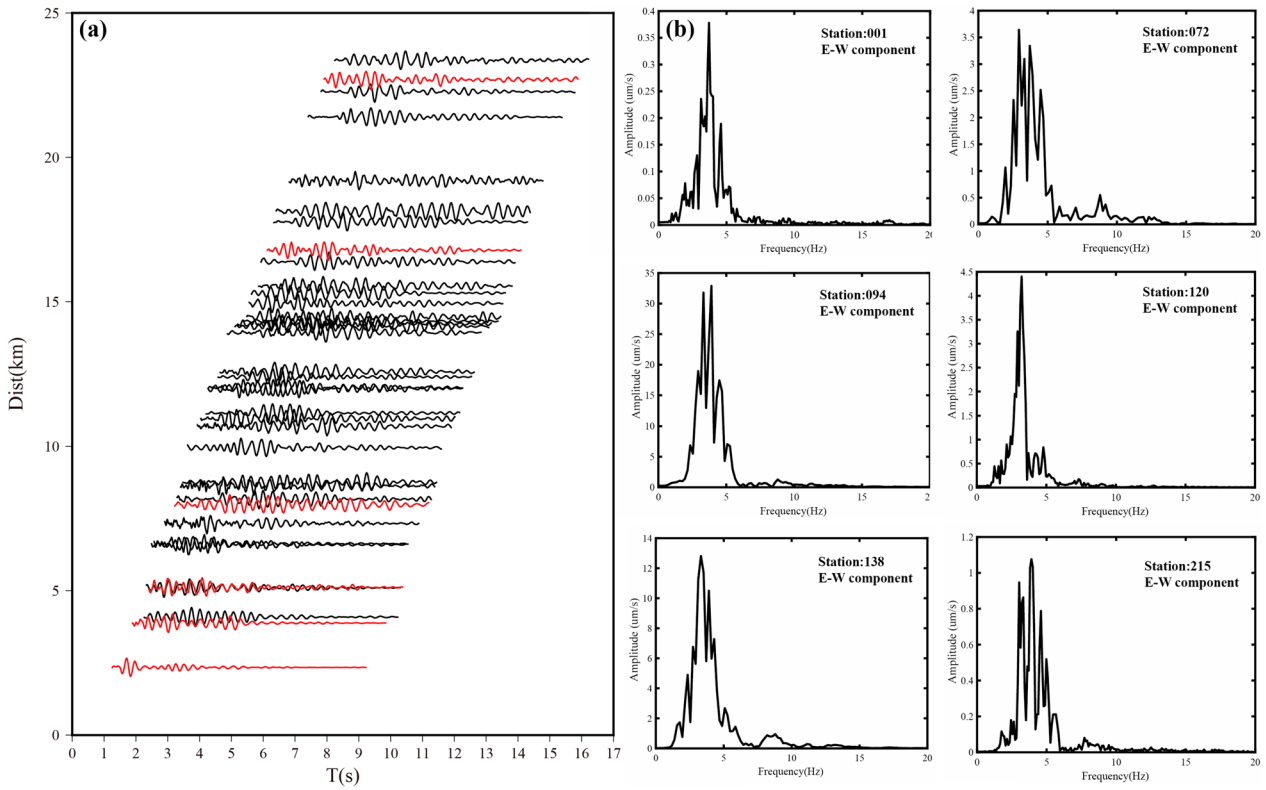

Fig. 5 Amplitude spectra of six stations. The waveform in an 8-s time window starting from the onset of S wave is shown on the left, and the amplitude spectra of six stations is displayed on the right. The waveform of the amplitude spectra in **b** is indicated in red in **a**

quality factor Q_s^{-1} was calculated from the coefficient b (Eq. 2).

Coda normalization method

To evaluate frequency-dependent Q using the coda normalization method, we analyzed the signals by using a four-pole Butterworth filter with a center frequency of 2, 3, 4, 5, 6 Hz and $\pm\frac{f}{3}$ bandwidth and obtained the traces in these five frequency bands (Fig. 6). On the filtered seismograms, we measured the RMS amplitude of the S wave $As(f,r)$ (Eq. 4) in an 8-s time window starting from the arrival of the S wave. We then measured the coda spectral amplitude $Ac(f,t_c)$ from the RMS coda amplitude in each frequency band. The lapse time used to calculate $Ac(f,t_c)$ is usually greater than twice the S wave traveltime. In this study, the S-wave traveltime at the farthest station is approximately 8.24 s, so $Ac(f,t_c)$ was calculated for a 5-s time window at $t_c = 17$ s, where the lapse time t_c is measured from the origin time. We substituted these observed values into Eq. 8 and estimated Q_s^{-1} by means of the least-squares method, taking the S-wave velocity as 2.87 km/s. The frequency dependence of Q_s^{-1} can be obtained from the center frequencies of different frequency bands and the corresponding Q_s^{-1} values. The epicentral distance of the stations selected in this study ranged from 2.3 to 23.4 km, with a wide range of epicentral distances. For stations with small epicentral distance, the coda amplitude may be lower than the noise level, or even the signal has completely disappeared when $t_c = 17$ s. It is necessary to use a value predicted for $t_c = 17$ s from coda-amplitude measurement at an earlier lapse time. For that purpose, we made a master curve for the decay of coda amplitude against lapse time (Aki and Chouet 1975; Aki 1980a; Yoshimoto et al. 1993, 1998). For the stations with epicentral distance less than 5 km, we measured the RMS amplitude $Ac(f,t_{c1})$ in a 3 s time window at $t_{c1} = 8$ s and $As(f,r)$ was calculated in a 5 s window. We measured the RMS amplitude $Ac(f,t_{c1})$ in a 3 s time window at $t_{c1} = 11$ s for stations with epicentral distance from 5 to 8 km. The measured values are reduced to $t_c = 17$ s by dividing by the factor $A_{c1}(f,t_{c1})/A_c(f,t_c = 17s)$ (Table 1).

However, since little research has been conducted on the coda waves produced by an airgun source, it is necessary to check whether the selected signal is a coda wave after determining the signal window. On the basis of laboratory ultrasonic measurements, Guo et al. (2009) reported that the amplitude of the coda wave conforms to a linear attenuation relationship with time. Sato (1977)

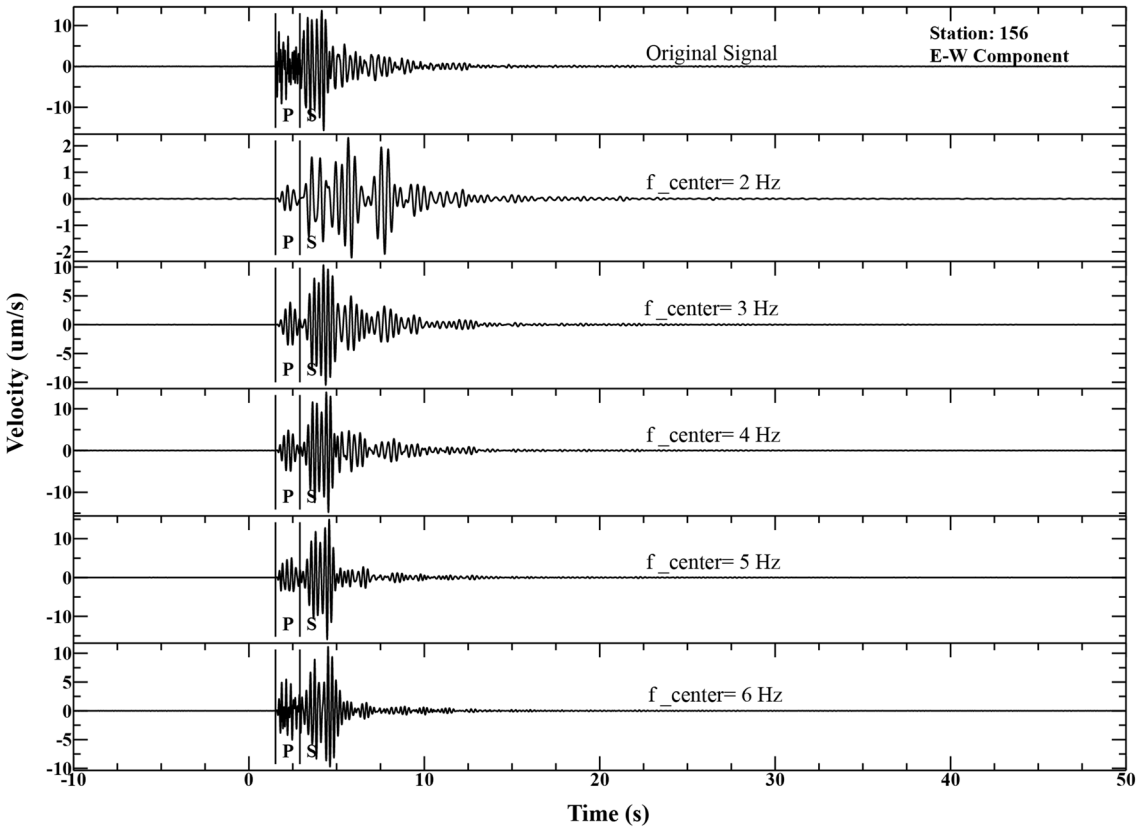

Fig. 6 Traces of the original signal and the filtered waveforms at five center frequencies. The vertical axis shows the velocity in um/s and horizontal axis indicates time in s

Table 1 The values of $A_{c1}(f, t_{c1})/A_c(f, t_c = 17s)$ at different center frequencies

Station	t_{c1}	Frequency				
		2 Hz	3 Hz	4 Hz	5 Hz	6 Hz
94	$t_{c1} = 8$ s	11.21	17.71	31.39	40.41	32.79
138		31.39	49.17	53.79	27.78	30.10
97		20.40	32.79	45.17	66.81	78.51
135	$t_{c1} = 11$ s	6.59	4.40	5.32	5.52	6.24
72		5.94	8.58	6.59	6.90	4.17
113		3.57	3.97	4.61	5.43	5.51
156		5.02	6.14	4.84	4.57	4.17
51		4.06	8.58	5.94	6.90	5.51

derived the following energy density equation from a single isotropic scattering model considering the case of a non-coincident source and receiver:

$$E(x,t) = \frac{W(\omega)g_0(\omega)}{4\pi r^2} K\left(\frac{V_0 t}{r}\right) H(V_0 t - r) e^{-Q_c^{-1}\omega t}, \tag{12}$$

where W is the total seismic energy generated by the earthquake within the unit frequency band around ω, $g_0(\omega)$ is the total scattering coefficient, V_0 is the wave velocity, t is the lapse time, and H is the step function. The function $K(\nu)$ is given by:

$$K(\nu) = \int_{-1}^{1} d\omega \frac{1}{\nu^2 - \omega^2} = \frac{2}{\nu} \tanh^{-1}\frac{1}{\nu} = \frac{1}{\nu} \ln\frac{\nu+1}{\nu-1} \nu > 1. \tag{13}$$

Because the product of the wave velocity V_0 and lapse time satisfies $V_0 t > r$, the coda energy density at frequency f can be expressed as:

$$E(f|r,t) = \frac{W(f)g_0(f)}{4\pi r^2} K(a) e^{-2Q_c^{-1}\pi f t}, \tag{14}$$

where r is the hypocentral distance, t is the lapse time measured from the origin time of the earthquake, $K(a) = \frac{1}{a}\ln\frac{a+1}{a-1}$, and $a = \frac{t}{t_s}$. The energy density is proportional to the RMS amplitudes of coda waves. Equation 14 can be taken as a natural logarithm, and these terms can be rearranged:

$$\ln\left[\frac{A(f|r,t)}{K(r,a)}\right] = \ln C(f) - \left(\frac{\pi f}{Q_c}\right)t, \tag{15}$$

where $A(f|r,t)$ represents the observed RMS amplitudes of the bandpass-filtered waveforms with center frequency f, $K(r,a) = \frac{1}{r}K(a)^{0.5}$ and $C(f)$ is a constant. Hence, if the attenuation of coda waves is a straight line fitting the measured $\ln[\frac{A_{obs}(f|r,t)}{K(r,a)}]$ versus t for a given center frequency, we can conclude that the signal is a coda wave. According to the above method to verify the recorded signal, the amplitude varies linearly with time (Fig. 7), guaranteeing that a coda wave has been selected.

Results

Amplitude–distance attenuation method

On the basis of the Yamaoka amplitude–distance attenuation method introduced in the second part, the curve of the amplitude spectrum versus distance was obtained by fitting (Fig. 8). The normalized values of the amplitude–distance spectra in both EW and NS components (except for station No. 97 at 4.1 km) satisfy the power exponential decay relationship plotted in Fig. 8. In the Up–Down (UD) component, the deviation of station No. 97 from the fitting curve is much smaller than that of the EW and NS components. The frequency corresponding to the amplitude of each station is calculated by Eq. 3 (Table 2), and the average frequency is approximately 3.6 Hz. These parameters provide the Q_s^{-1} values of the three components are 0.0260 ± 0.0103, 0.0264 ± 0.0109, 0.0256 ± 0.0080, respectively. The Q_s^{-1} value of EW component is almost equal to the value of NS component, which further proves that the amplitude of the two components is not significantly different. Therefore, we only use the EW component for the S-wave analysis in the following study.

Coda normalization method

Using the coda normalization method, we applied a four-pole Butterworth filter with a center frequency of 2, 3, 4, 5, 6 Hz to the waveform and calculated the RMS

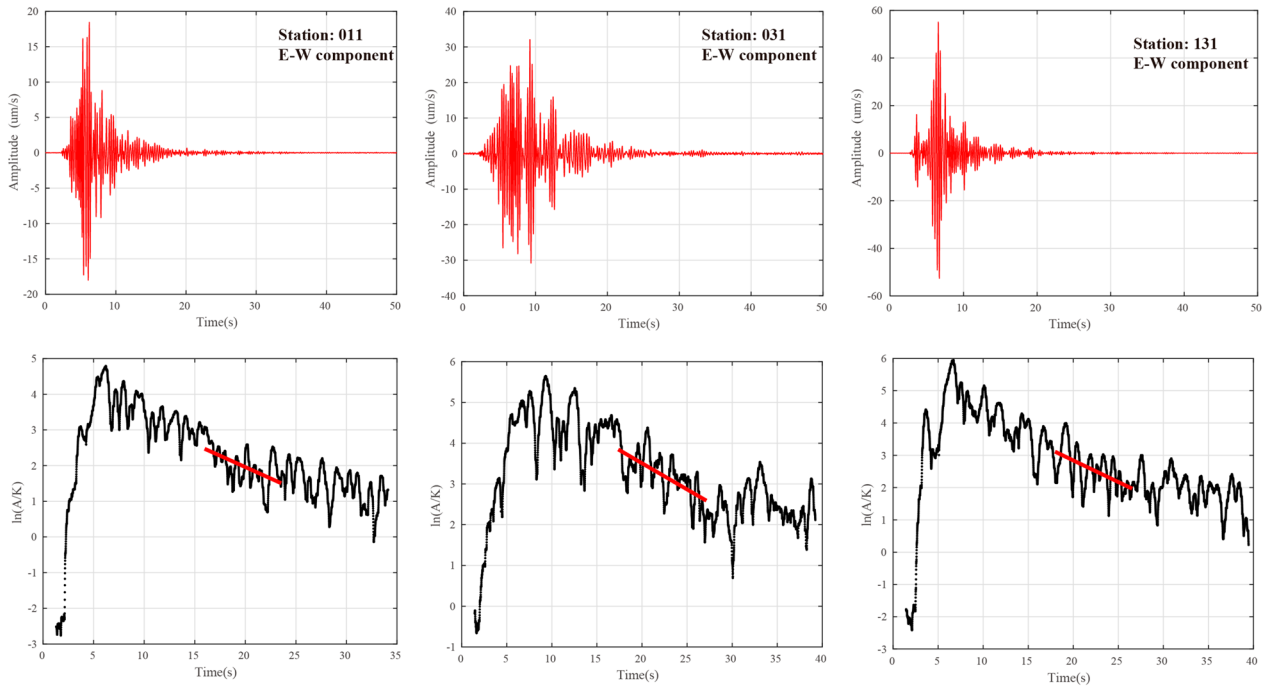

Fig. 7 The function $\ln[A(f|r,t)/K(r,a)]$ versus lapse time t of the selected coda windows at three stations. Coda waves are shown in red in the upper graph, and the lower graphs illustrate the relationship that the function $\ln[A(f|r,t)/K(r,a)]$ versus lapse time t along with least-squares fits of selected signal windows

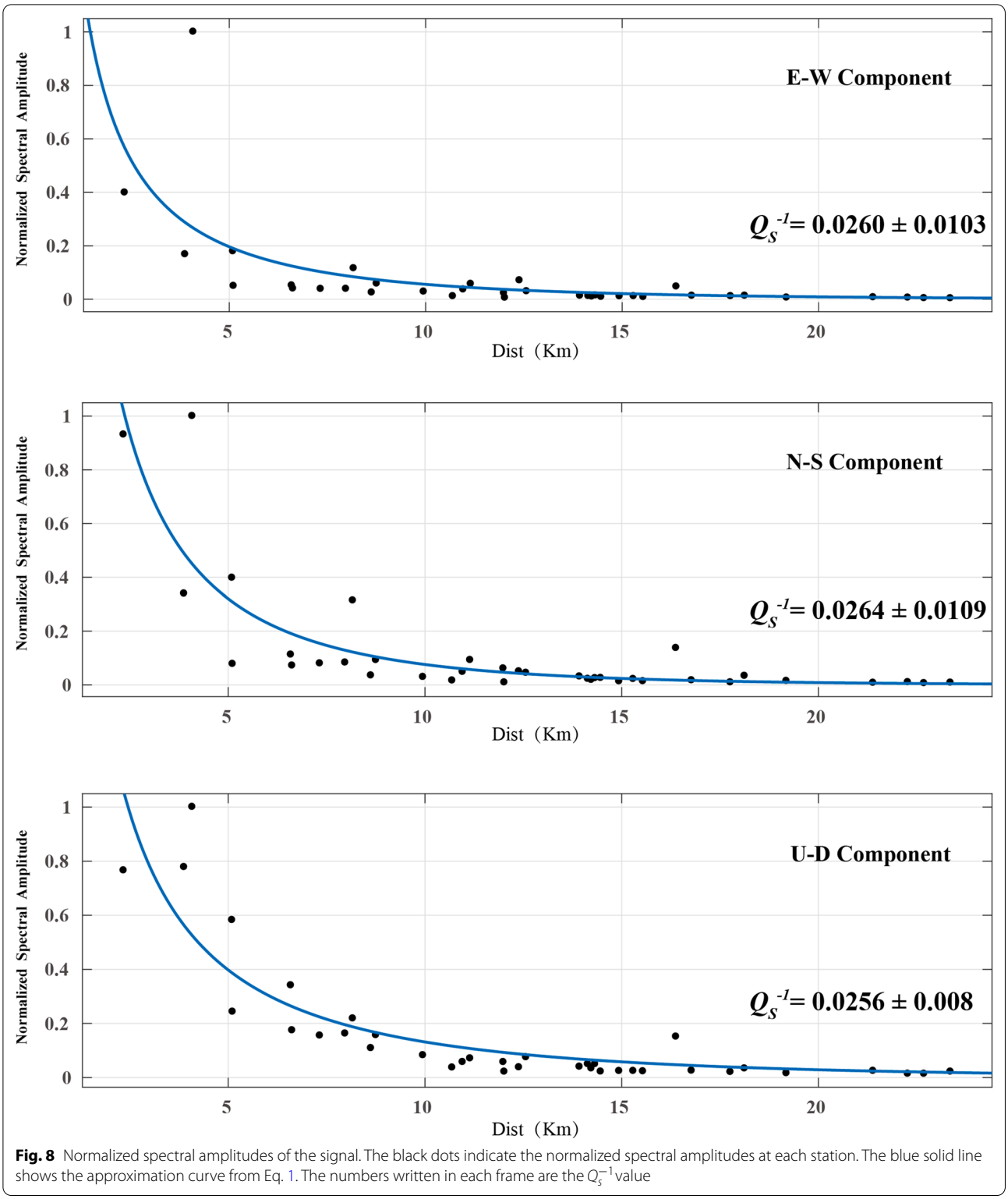

Fig. 8 Normalized spectral amplitudes of the signal. The black dots indicate the normalized spectral amplitudes at each station. The blue solid line shows the approximation curve from Eq. 1. The numbers written in each frame are the Q_s^{-1} value

amplitudes of the recorded signals. The coda-normalized amplitudes of the S wave against the hypocentral distance for each frequency band are plotted in Fig. 9, and least-squares line were fitted to the data in all frequency bands. The Q_s^{-1} value at the center frequency of 2 Hz is approximately 0.0365 ± 0.0205, and the value is 0.0313

Table 2 The frequency corresponding to the amplitude spectrum of 37 stations (EW component)

Station	Frequency (Hz)	Station	Frequency (Hz)	Station	Frequency (Hz)	Station	Frequency (Hz)
1	3.749	51	3.654	113	3.628	174	3.387
6	3.730	56	3.520	120	3.332	181	3.636
11	3.767	61	3.529	122	3.345	185	3.413
16	3.682	66	3.570	131	3.577	198	3.758
21	3.608	72	3.664	135	3.509	202	3.442
26	3.845	81	3.488	138	3.630	215	3.969
31	3.654	94	3.750	146	3.494	231	3.599
36	3.515	97	3.785	151	3.282		
42	3.618	101	3.727	156	3.854	Average	3.611
46	3.709	107	3.305	170	3.882		

$\pm$ 0.0133 at center frequency of 3 Hz, while those at the center frequencies of 4, 5, 6 Hz are 0.0257 $\pm$ 0.0101, 0.0228 $\pm$ 0.0086 and 0.0186 $\pm$ 0.0070, respectively. The coda-normalized amplitude attenuation curves in the five frequency bands with distance (Fig. 9) reveal that scatter in data points around the fitting line is relatively small for all frequency bands, but we see a tendency that the scatter at low frequencies is slightly larger than that at high frequencies. The values of Q_s^{-1} decrease with increasing frequency from about 0.0365 at 2 Hz to 0.0186

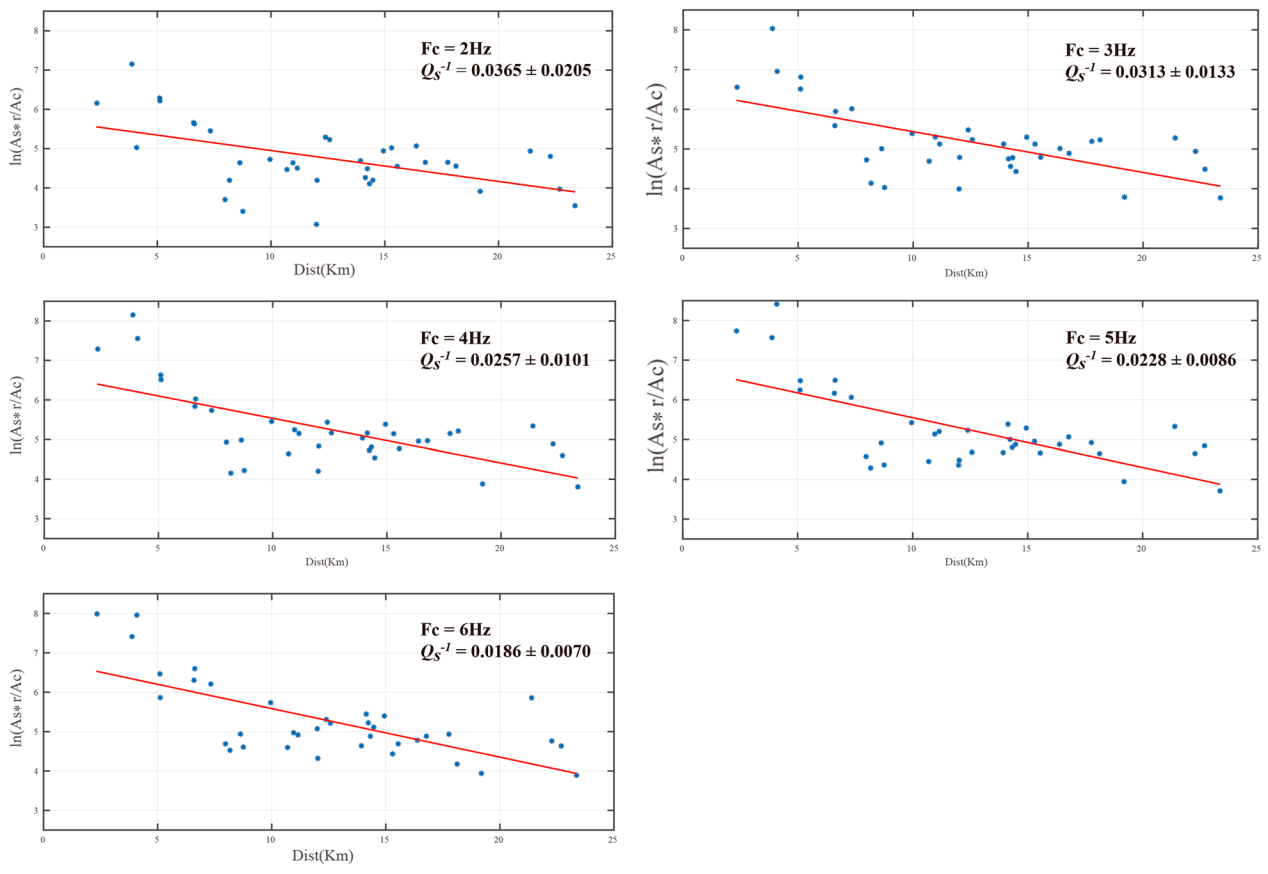

Fig. 9 Coda-normalized RMS amplitude decay of S waves with hypocentral distance. The solid red lines indicate the least-squares fitting curves. The numbers written in each frame are the Q_s^{-1} value and its corresponding center frequency

at 6 Hz. The center frequencies of the five frequency bands and their corresponding Q_s^{-1} values were fitted by the power law mentioned in part 2, and the relationship between the Q_s^{-1} value and the frequency was obtained as $Q_s^{-1}(f) \cong 0.0554 f^{-0.5643}$. Substituting the frequency (3.6 Hz) used in the amplitude–distance decay method into the aforementioned equation, $Q_s^{-1}(3.6) = 0.0269$. Due to the small footprint of the dense seismic array with an airgun source, the information reflected by the signal pertains mainly to the shallow media, and thus, the calculation of the Q_s^{-1} value is volatile. Therefore, we assert that the Q_s^{-1} values calculated by the Yamaoka amplitude–distance attenuation method and the Aki coda normalization method are consistent.

Discussion

Impact of data fluctuations on the results

The results of these two methods contain points that deviate greatly from the fitted curve, and these anomalous data have considerable impacts on the accuracy and stability of the fitting results. In the results of Yamaoka's amplitude–distance attenuation method, the amplitude recorded by station No. 97 at a distance of 4.1 km from the epicenter is much larger than the corresponding amplitude on the fitted curve. To reduce the influence of this point on the fitting result, station No. 97 was eliminated, and the fit was performed again to obtain a new amplitude attenuation curve (Fig. 10). The normalized spectral amplitude of the S waves received by the remaining 36 stations decays into a power exponential relation with distance, and the normalized amplitudes are distributed around the fitted curve. However, 4 among the 36 stations continue to exhibit large deviations from the fitted curve, namely, stations No. 135, 56, 131, and 66 in order of increasing hypocentral distance. Compared with that of station No. 97, the deviations of these 4 stations from the curve are smaller. The Q_s^{-1} value obtained by fitting the new curve is approximately 0.0221 ± 0.0094, which is 15% different from the initial results.

The amplitude distribution in the low-frequency (2 Hz) obtained by the coda normalization method is more discrete than the distributions in the other four frequency bands. Five stations display relatively large deviations from the fitted curve, namely, stations No. 138, 120, 56, 31 and 101 (Fig. 11), one of which also appear as outliers in the results of the amplitude–distance attenuation method (stations No. 56). To test the influence of these anomalous stations on the results, we removed them and recalculated the Q_s^{-1} value to obtain the results shown in Fig. 12. The fitting results after removing these anomalous stations have better linear attenuation relations than the results plotted in Fig. 9, especially the data distribution at the center frequency of 2 Hz, which is more convergent. The Q_s^{-1} values obtained by the new fitted curves are changed relative to the previous value with a change range of 1.9%~7.5%; this difference is caused mainly by the data at 2 Hz center frequency. Adopting a frequency-dependent power law, we obtain a new relation: $Q_s^{-1} = 0.0581 f^{-0.5668}$.

From the comparison of these two methods, the Yamaoka amplitude–distance attenuation method is relatively unstable, and the variation in the RMS amplitude of each station has a greater impact on the fitting results. In contrast, since the coda normalization method uses the ratio of S and coda spectra recorded by the same station, the results are relatively stable. In addition, the Q_s^{-1} value is related to the epicentral distance of the data used (Kumar et al. 2005; Sharma et al. 2007; Hua et al. 2009): the

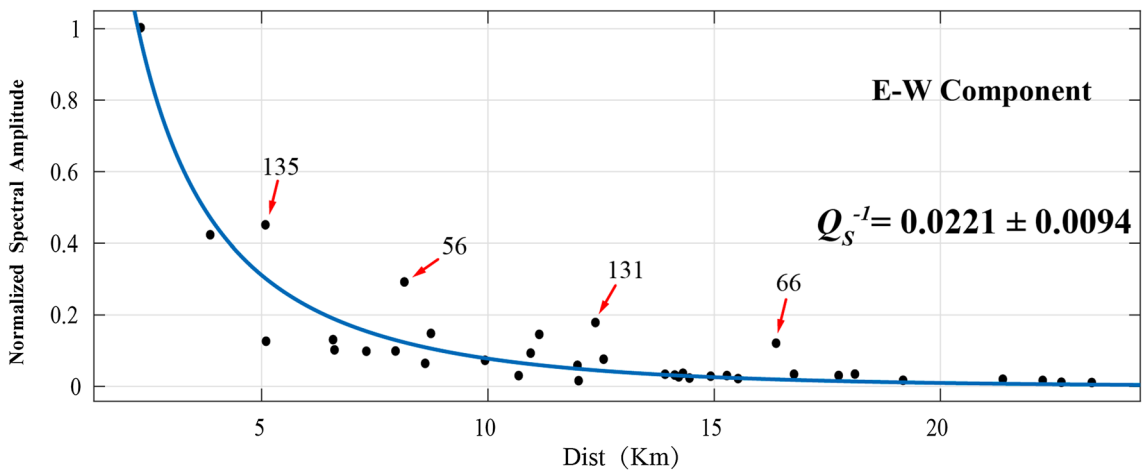

Fig. 10 Normalized spectral amplitude attenuation curve of S waves. The red arrows mark the numbers of the 4 anomalous stations

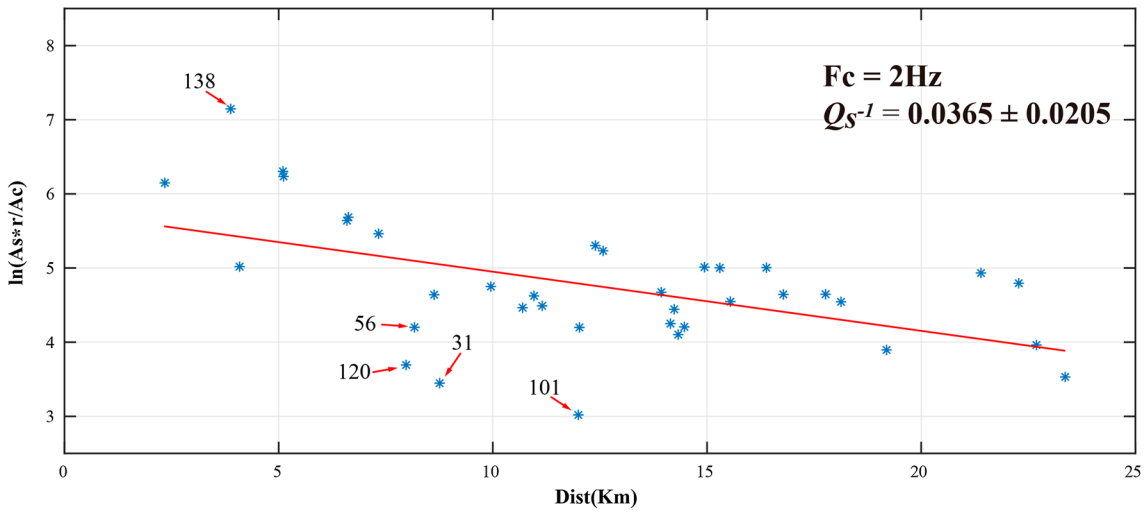

Fig. 11 Schematic diagram of anomalous coda-normalized points

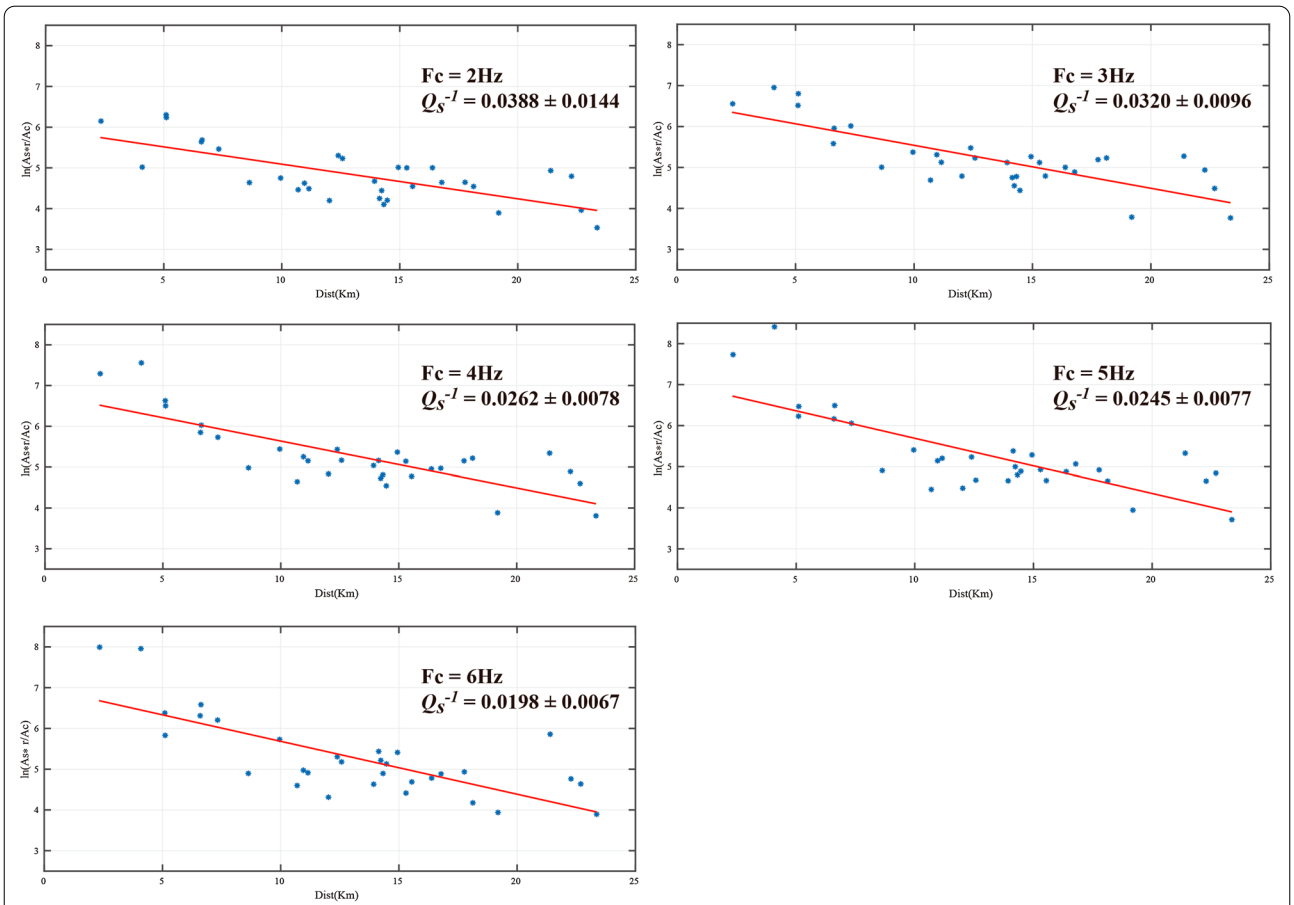

Fig. 12 Coda-normalized RMS amplitude decay of S waves with hypocentral distance after removing anomalous stations. The red solid lines indicate least-squares fits of all stations. The numbers written in each frame are the Q_s^{-1} values

greater the epicentral distance is, the greater the depth of wave penetration and the smaller the Q_s^{-1} value. The dense seismic array with an airgun source used in this study was arranged in a small area, and the maximum epicentral distance was 23.4 km; hence, the information extracted from these seismic data pertains mainly to the shallow subsurface media, and thus, the corresponding Q_s^{-1} value is large. However, due to the effects of the shallow sedimentary layer and topography, the Q_s^{-1} value is prone to large changes. This requires us to not only use high-precision wave data for the calculation, but also consider the influences of terrain and the sedimentary cover. Hence, areas with large changes in the sedimentary thickness or topography should be divided into different areas for the calculation to reduce deviation.

Relation between anomalous points and topography

The Binchuan area is located at the junction of the Central Yunnan Plateau and the Hengduan Mountains. Consequently, the terrain reaches high elevations both to the east and to the west, whereas the topography is low in the middle, yielding a relative elevation difference of up to 2000 m. To the east of the F1 fault on the eastern side of the Binchuan Basin (Fig. 13) is the Dongshan Mountain Range with a maximum elevation of 2866 m, while the average elevation of the Piedmont Basin on the western side of F1 drops to approximately 1500 m (Luo et al. 2015); accordingly, the study area is characterized by rugged terrain. The anomalous stations detected in the results of the Yamaoka amplitude–distance attenuation method and Aki coda normalization method are emphasized in Fig. 14 to explore the relationship between the anomalous spectral amplitudes and the topography. The red triangle in Fig. 14 is the anomalous station in both methods, the white triangles are the anomalous stations unique to the amplitude–distance attenuation method, and the four black triangles are the anomalous stations unique to the coda normalization method.

As shown by the station distribution in Fig. 14, red station is located in the Binchuan Basin underlain by thick sediments, while station No. 131 and 66 are located in the hilly area on the western side of the basin. The four black stations and station No. 135 are located inside the Binchuan Basin and on the edge of the basin. Studies have shown that the basin has a significant impact on the intensity of the seismic response; in particular, stations on the edge and within the center of the basin experience strong edge effect and amplification effect (Adams 2000; Qiang 2020). Specifically, seismic waves traveling to the edge of the basin encounter the mountain range, which acts as an interface and reflects part of the waves, superimposing the wavefield and resulting in stronger seismic waves at the edge of the basin. These waves are then reflected and refracted multiple times within the basin and resonate within the sedimentary cover, which strengthens the energy of low-frequency ground motions. Station No. 135 (white triangle) is located at the edge of the basin, and the amplitude is larger than the fitted curve due to the basin edge effect. In the coda normalization method, stations No. 101 and 31 located at the edge of the basin are influenced by the basin effect that produces a superimposed wavefield and directly effects the coda wave amplitude; thus, $Ac(f,t_c)$ is greater than the theoretical value, causing $\ln\frac{As(f,r)r}{Ac(f,t_c)}$ to be smaller than normal. The $Ac(f,t_c)$ of station No. 138 needs to be converted by dividing by $A_{c1}(f,t_{c1})/A_c(f,t_c)$, which may introduce errors to make $Ac(f,t_c)$ smaller, resulting in $\ln\frac{As(f,r)r}{Ac(f,t_c)}$ larger. Sun (2019) studied the sedimentary layer thickness in the Binchuan Basin and reported two depocenters in the basin, namely, the Binchuan depocenter in the north and the Binju depocenter in the south (Fig. 15). A comparison of Figs. 14 and 15 suggests that stations No. 56 (red triangles) and station No. 120 (black triangle) are located inside the Binchuan depocenter. In order to explore the effect of the amplification effect inside the basin on these two stations, the resonance frequency of the basin is calculated. The thickness of the sedimentary layer at the edge of Binchuan depocenter is about 350 m, and the shear wave velocity in the basin is approximately 500 m/s (Yang et al. 2020). The relationship between resonance frequency and thickness of sedimentary layer can be expressed as follows (Seht and Wohlenberg 1999):

$$f_R = \frac{v_s}{4m}, \tag{16}$$

where v_s is shear wave velocity and m indicates sediment thickness. It can be concluded that the resonance frequency in the basin is approximately 0.36 Hz based on Eq. 16, which is quite different from the abnormal frequency band (2 Hz) of stations. The influence of the basin amplification effect can be excluded. Therefore, we speculate that the local site factors may be the cause of the deviation of the spectral amplitudes at these stations from the fitted curve. This inference needs to be further studied in the follow-up work due to the lack of site data.

Furthermore, stations No. 131 and 66 are located in hilly areas, where the shallow structure has a smaller porosity and is harder than a soft-soiled basin; thus, the waves passing through these areas experience less attenuation, increasing the RMS amplitudes of the direct waves reaching these two stations. However, since this feasibility study selected only some stations from the dense array, the relation between the amplitude and topography needs to be further explored in subsequent studies.

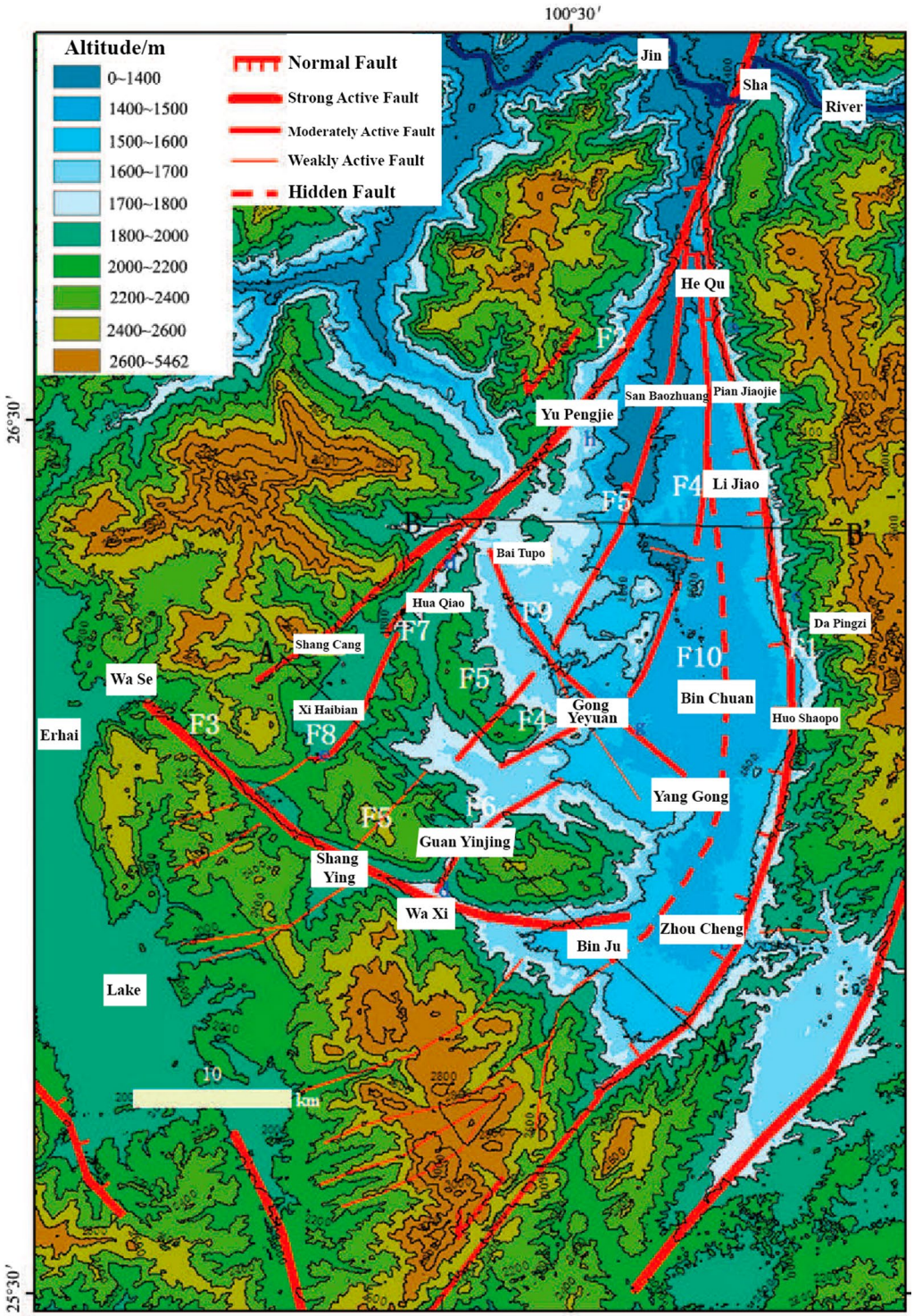

Fig. 13 Topographic map of the Binchuan area (Luo et al. 2015). F1–F9 represent Binchuan Fault, Shangcang-Yupeng Fault, Binju Fault, Pianjiao-Daying Fault, Hequ-Shangying Fault, Zhouchengxi Fault, Huaqiao Fault, Xihaibian Fault, and Baitupo-Yanggongcun Fault, respectively. F10 indicates a hidden fault

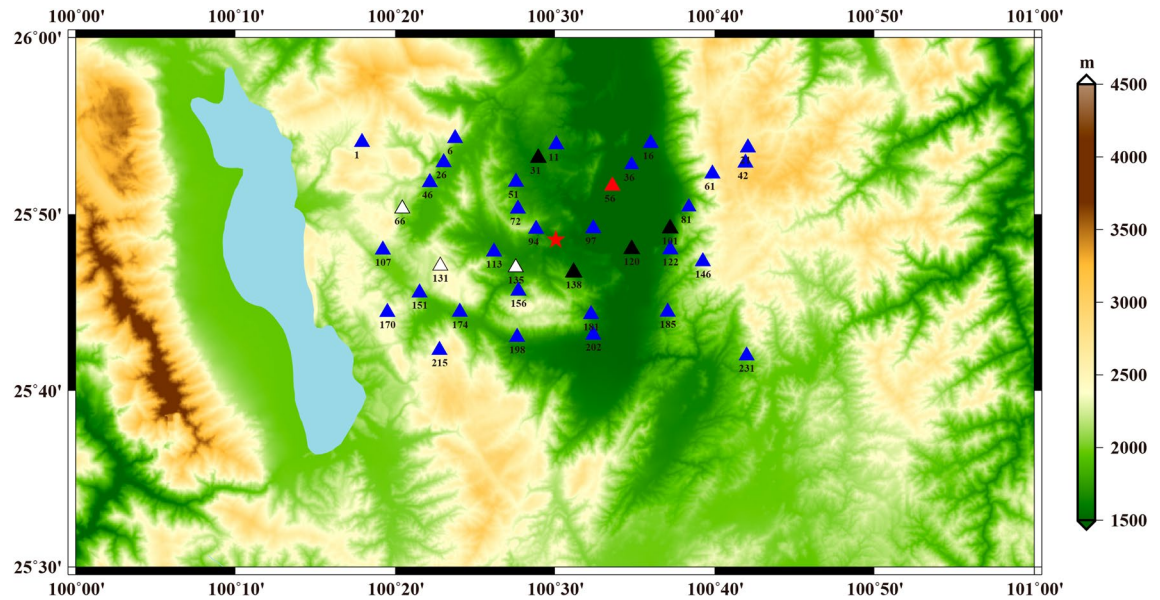

Fig. 14 Distribution of anomalous stations. The red triangle is the anomalous station in both methods, the white triangles are the anomalous stations unique to the amplitude–distance attenuation method, the black triangles are the anomalous stations unique to the coda normalization method

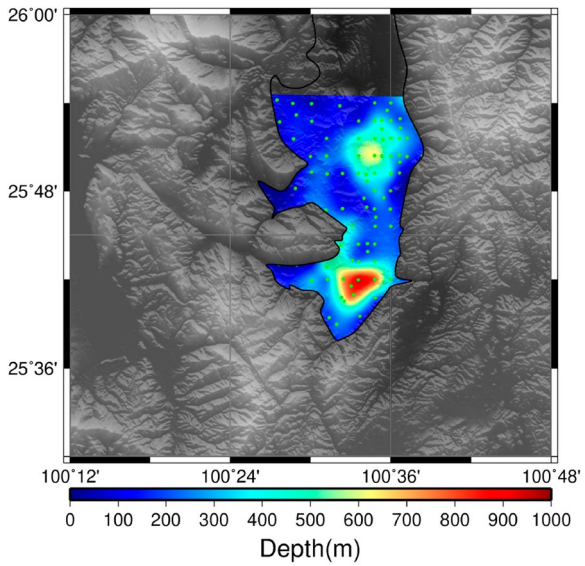

Fig. 15 Thickness of the sedimentary layer in the Binchuan Basin (Sun 2019). The green dots are the stations used in the calculation

Comparison with other regions

Wang et al. (2005) used six seismic stations in Yunnan Province, China, to obtain the S-wave attenuation in this region by using the coda normalization method. They divided the stations into 3 research areas: research area 1, where the Baoshan (BS) station is located; research area 2, where the Yongsheng (YS), Lijiang (LJ), and Heqing (HQ) stations are located; and research area 3, where the Luquan (LQ) and Yimen (YM) stations are located (see Additional file 1, Fig. S2). The relationships between Q_s^{-1} and frequency in these three areas can be expressed as $Q_s^{-1} = 0.00867f^{-0.86}$, $Q_s^{-1} = 0.01824f^{-0.94}$, and $Q_s^{-1} = 0.01647f^{-0.91}$. Figure 16a shows a comparison between the Q_s^{-1} of the three areas and the Q_s^{-1} estimated in this study. The study area is located at the junction of research area 1 and research area 2 (the northeastern part of area 1 and the southern part of area 2). Since Wang et al. (2005) used natural seismic data, compared with the airgun source, their result reflects the Q_s^{-1} value of the deeper medium, which is generally smaller than the Q_s^{-1} value of this study. In addition, there is only one airgun source in this study, and the error of the fitting results is much larger than that of natural earthquakes, which needs to be improved in our following study. Therefore, we believe that the results of this study are consistent with the actual situation of the shallow medium in the Binchuan area.

Yoshimoto (1993) used the coda normalization method to estimate the Q_s^{-1} value in the Kanto region of Japan, and Mamada and Takenaka (2004) obtained the Q_s^{-1} inside and outside the focal region of the 1997 northwestern Kagoshima earthquake by using the same method. Satoh (2006) used surface and borehole seismic data to invert the Q_s^{-1} value in the Sendai Basin, Japan, and obtained the Q_s^{-1} variation relationship with different sedimentary structures. Wang and Li (2018) inverted

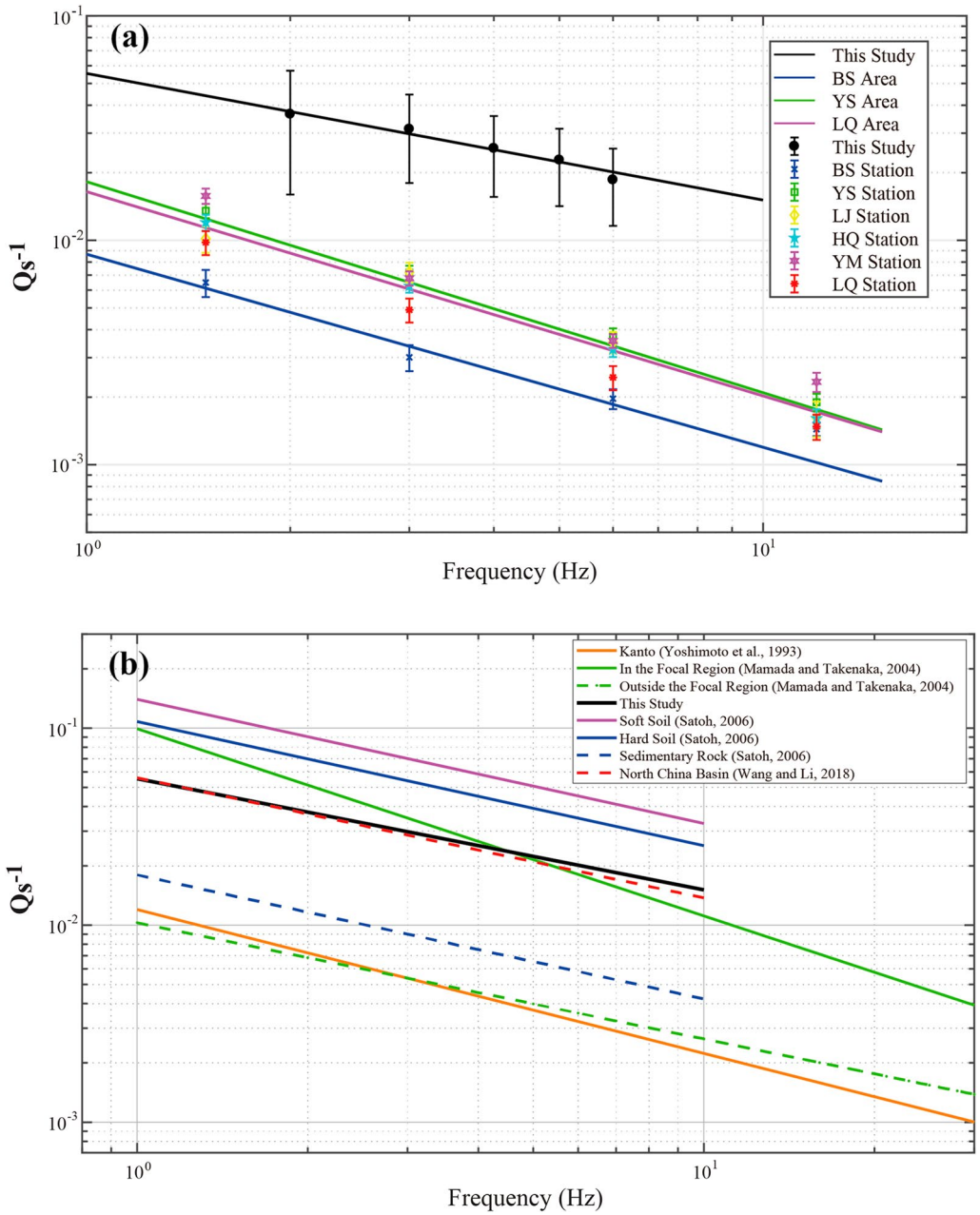

Fig. 16 Comparison with previous research results. **a** Is the comparison with the results of adjacent areas. The results of the present study are plotted by black solid circles. The error bar indicates the fitting deviation. The solid black line is the curve of Q_s^{-1} versus frequency obtained in this study. The blue crosses, green squares, yellow diamonds, bright blue pentagrams, magenta hexagrams and red stars show the Q_s^{-1} value of BS station, YS station, LJ station, HQ station, YM station and LQ station, respectively (Wang et al. 2005). **b** Is a comparison of the power law decaying model for Q_s^{-1} in different areas and rock types. The black solid line is the result for our study. The orange solid line, green solid line and green dash line show the result in the Kanto area (Yoshimoto et al. 1993), in the focal region and outside the focal region (Mamada and Takenaka 2004), respectively. The magenta line, blue solid line and blue dash line are the Q_s^{-1} model for shallow structure of soft soil, hard soil and sedimentary rock (Satoh 2006). The red dash line indicates the decaying model in the North China Basin (Wang and Li 2018)

the S-wave attenuation of shallow sedimentary layers in the North China Basin based on near-seismic borehole data. Comparing these results with the findings in this study (Fig. 16b), the Q_s^{-1} obtained from far-field natural earthquakes mainly reflects the deep features of the Earth and is much smaller than the downhole and near-field data. Comparing the results with those for different rock types calculated by Satoh (2006), the Q_s^{-1} value estimated

in this study is between the values for hard soil and sedimentary rocks and is similar to the Q_s^{-1} obtained by Wang and Li (2018) in the North China Basin. These comparisons further demonstrate the rationality and accuracy of the results of this study.

Zhang et al. (2020) inverted the three-dimensional velocity structure of Binchuan area, and the results showed that the overall velocity of the region was relatively low at the depth of 0 km, only the hilly regions in the west and southwest direction had high velocity (see Additional file 1: Fig. S3). The wave speed is consistent with the Q value. Loose media structures result in lower wave velocities and higher attenuation, which means the value of Q_s^{-1} is larger. Compared with the results of natural earthquakes, the Q_s^{-1} in our study is larger, which corresponds to the velocity characteristics obtained by Zhang et al. (2020).

Conclusion

Based on the data from 37 seismic stations uniformly selected from a dense array with an airgun source in Binchuan, Yunnan Province, China, this paper applies the Yamaoka amplitude–distance attenuation method and the Aki coda normalization method to explore the feasibility of utilizing an airgun source for calculating the Q_s^{-1} values of shallow media. In summary, a comparison of the calculation results of the two methods confirms that an airgun seismic source can be used to detect the Q_s^{-1} values of shallow media, and the results are stable and consistent with the actual situation.

However, some points exhibit large deviations from the fitted curve in the two results. After removing these abnormal points and refitting the normalized amplitudes, it is found that the abnormal points have different effects on the two methods. Since the coda normalization method uses the ratio of the S wave to coda wave spectra recorded by the same station, it reduces the influence of abnormal points on the fitted Q_s^{-1} values to a certain extent, so the stability of the coda normalization method is higher than that of the Yamaoka amplitude–distance attenuation method. Moreover, considering the small coverage of the dense array, the results represent mainly shallow media, so the Q_s^{-1} value is large and is greatly affected by both the topography and the sedimentary cover. We assert that the calculation results of these two methods are consistent with the actual situation. Given the topography, we speculate that the anomalous stations located on the edge of the Binchuan Basin and in the western hilly area are due to the edge effect of the basin and the weak attenuation of the hilly area, and the anomalous station located in the northern Binchuan depocenter are attributable to local site factors, which need to be further verified in a following study using data from the entire dense array. Compared with the Q_s^{-1} estimated by previous studies, the Q_s^{-1} in the Binchuan area is found to lie between those of the hard soil and sedimentary rock and is similar to the Q_s^{-1} in the North China Basin. It corresponds to the shallow velocity structure in this area, and further proves the rationality and accuracy of the Q_s^{-1} estimated in our study.

Abbreviations

PGA: Peak ground acceleration; Sa: Response spectrum; SNR: Signal-to-noise-ratio; ACROSS: Accurately Controlled Routinely Operated Signal System; RMS: Root mean square; EW: East–West; 1-D: One-dimensional; NS: North–South; BS: Baoshan; YS: Yongsheng; LJ: Lijiang; HQ: Heqing; LQ: Luquan; YM: Yimen.

Supplementary Information

The online version contains supplementary material available at https://doi.org/10.1186/s40623-022-01625-2.

Additional file 1: Figure S1. Spatial distribution of airgun signal intensity (Jiang 2017). **Figure S2.** Distribution of research areas (Wang et al. 2005). **Figure S3.** Three Dimensional structure in Binchuan area (Zhang et al. 2020).

Acknowledgements

Seismic data used in this study were collected during the experiment of imaging the Binchuan basin with active sources cooperatively by the Institute of Geophysics, China Earthquake Administration (IGP-CEA), the Geophysical Exploration Center, China Earthquake Administration (GEC-CEA), the Earthquake Agency of Yunnan Province (EAY) and ChenYong Workgroup of Yunnan province (No. 2014IC007). We are grateful to Dr. Yunpeng Zhang, Dr. Jinbo Su and Dr. Feng Gao for valuable comments and discussion. We thank the editor and two anonymous reviewers for their constructive, helpful and positive comments that significantly improved the paper.

Author contributions

SD carried out the analyses, interpreted the results and drafted the manuscript. YXY guided the study and gave useful advice about the results. LX took part in the design of the study. All authors read and approved the final manuscript.

Funding

This work was supported jointly by the National Key R&D Program of China (Grant Number 2020YFA0710603), the National Natural Science Foundation of China (Grant Numbers 41974069 and 41790463), and the Basic R&D Operations Special Fund of the Institute of Geophysics, China Earthquake Administration (Grant Number DQJB21Z09).

Availability of data and materials

The stacked airgun waveforms using in current study can be accessed from the corresponding author YanXiang Yu under request.

Declarations

Ethics approval and consent to participate

Not applicable.

Consent for publication

Not applicable.

Competing interests

The authors declare that they have no competing interests.

Received: 7 November 2021 Accepted: 6 April 2022
Published online: 07 May 2022

References

Adams BM (2000) Basin-edge effects from SH-wave modeling with reference to the Lower Hutt Valley, New Zealand. Dissertation, University of Canterbury Christchurch

Aki K (1969) Analysis of the seismic coda of local earthquakes as scattered waves. J Geophys Res 74(2):615–631. https://doi.org/10.1029/JB074i002p00615

Aki K (1980a) Attenuation of shear-waves in the lithosphere for frequencies from 0.05 to 25 Hz. Phys Earth Planet Inter 21:50–60

Aki K (1980b) Scattering and attenuation of shear waves in the lithosphere. J Geophys Res 86(B11):6496–6504. https://doi.org/10.1029/JB085iB11p06496

Aki K, Chouet B (1975) Origin of coda waves: source, attenuation, and scattering effects. J Geophys Res 80(23):3322–3342. https://doi.org/10.1029/JB080i023p03322

Aki K, Richards PG (1980) Quantitative seismology: theory and methods. Freeman W H, San Francisco

Anderson DL, Archambeau CB (1964) The anelasticity of the Earth. J Geophys Res 69(10):2071–2084. https://doi.org/10.1029/JZ069i010p02071

Battaglia J, Aki K (2003) Location of seismic events and eruptive fissures on the Piton de la Fournaise volcano using seismic amplitudes. J Geophys Res 108(B8):2364. https://doi.org/10.1029/2002JB002193

Caldwell J, Dragoset W (2000) A brief overview of seismic air-gun arrays. Lead Edge 19(8):898–902

Castro RR, Pacor F, Sala A, Petrungaro C (1996) S wave attenuation and site effects in the region of Friuli, Italy. J Geophys Res 101(10):22355–22369. https://doi.org/10.1029/96JB02295

Chen Y, Zhang X, Qiu X, Ge H, Liu B, Wang B (2007) A new way to generate seismic wave for continental crustal exploration. Chin Sci Bull 52(16):2264–2268. https://doi.org/10.1007/s11434-007-0247-4

Chen SW, Wang BS, Tian XF, Wang FY, Liu BF, Li L (2016) Crustal structure from Yunxian-Ninglang wide-angle seismic reflection and refraction profile in northwestern Yunnan, China. Seismol Geol 38(1):91–106. https://doi.org/10.3969/j.issn.0253-4967.2016.01.007

Drouet S, Souriau A, Cotton F (2005) Attenuation, seismic moments and site effects for weak-motion events: application to the Pyrenees. Bull Seismol Soc Am 95(5):1731–1748. https://doi.org/10.1785/0120040105

Guo MQ, Fu LY, Ba J (2009) Comparison of stress-associated coda attenuation and intrinsic attenuation from ultrasonic measurements. Geophys J Int 178(1):447–456. https://doi.org/10.1111/j.1365-246X.2009.04159.x

Hua W, Zhao C, Chen Z, Zheng S (2009) Attenuation of P, S and coda waves in Longtan reservoir region. Acta Seismol Sin 31(6):620–628. https://doi.org/10.3321/j.issn:0253-3782.2009.06.003

Jiang S (2017) Processing method and propagation characteristics of airgun source signals. Dissertation, Institute of Geophysics, China Earthquake Administration

Knopoff L (1964) Q. Rev Geophys. 2(4): 625–660

Kumar D, Sarkar I, Sriram V, Khattri KN (2005) Estimation of the source parameters of the Himalaya earthquake of October 19, 1991, average effective shear wave attenuation parameter and local site effects from accelerograms. Tectonophys 407:1–24. https://doi.org/10.1016/j.tecto.2005.06.006

Luo R, Wu Z, Huang X, Huang X, Zhou C, Tian T (2015) The main active faults and the active tectonic system of Binchuan area, northwestern Yunnan. Geol Bull China 34(1):155–170. https://doi.org/10.3969/j.issn.1671-2552.2015.01.013

Mamada Y, Takenaka H (2004) Strong attenuation of shear waves in the focal region of the 1997 northwestern Kagoshima Earthquakes, Japan. Bull Seismol Soc Am 94(2):464–478. https://doi.org/10.1785/0120030032

Niu F, Silver PG, Daley TM, Cheng X, Majer E (2008) Preseismic velocity changes observed from active source monitoring at the Parkfield SAFOD drill site. Nature 454:204–208. https://doi.org/10.1038/nature07111

Qiang S (2020) Research on the influencing factors of seismic response in two-dimensional basins. Dissertation, Institute of Engineering Mechanics, China Earthquake Administration

Sato H (1977) Energy propagation including scattering effects single isotropic scattering approximation. J Phys Earth 25(1):27–41. https://doi.org/10.4294/jpe1952.25.27

Satoh T (2006) Inversion of Qs of deep sediments from surface-to-borehole spectral ratios considering obliquely incident SH and SV waves. Bull Seismol Soc Am 96(3):943–956. https://doi.org/10.1785/0120040179

Seht M, Wohlenberg J (1999) Microtremor measurements used to map thickness of soft sediments. Bull Seismol Soc Am 89(1):250–259. https://doi.org/10.1785/BSSA08980010250

Sharma B, Teotia SS, Kumar D (2007) Attenuation of P, S, and coda waves in Koyna region, India. J Seismol 11:327–344. https://doi.org/10.1007/s10950-007-9057-z

Solomon SC, Toksöz MN (1970) Lateral variation of attenuation of P and S waves beneath the United States. Bull Seismol Soc Am 60(3):819–838. https://doi.org/10.1785/BSSA0600030819

Su JB, Wang BS, Wang HT, Wang Q, Ji ZB (2015) Research on characteristic of seismic attenuation in the Northern Tianshan Area using seismic signal from airgun source. J Seismol Res 38(4):598–605. https://doi.org/10.3969/j.issn.1000-0666.2015.04.011

Su Y (2009) Inversion tomography of the seismic wave attenuation (Q value) structure in Yunnan region. Dissertation, University of Science and Technology of China

Sun T (2019) Study on the sedimentary and crustal structures of the Binchuan Area using dense array. Dissertation, Institute of Geophysics, China Earthquake Administration

Wang S, Li Z (2018) S-wave attenuation of the shallow sediments in the North China basin based on borehole seismograms of local earthquakes. Geophys J Int 214:1391–1400. https://doi.org/10.1093/gji/ggy223

Wang Q, Liu J, Zheng S, Chen Z (2005) Frequency-dependent attenuation of P and S waves in Yunnan region. Acta Seismol Sin 27(6):588–597. https://doi.org/10.3321/j.issn:0253-3782.2005.06.002

Wang B, Wang W, Ge H, Xu P, Wang B (2011) Monitoring subsurface changes with active sources. Adv Earth Sci 26(3):249–256

Wang Z (2017) Research on stochastic simulation method for high frequency of ground motions. Dissertation, Institute of Engineering Mechanics, China Earthquake Administration

Wang Z, Zhao P, Bo J (2017) Analysis for the effects of main parameters on ground motions by stochastic simulation method. World Earthq Eng 33(3):34–41

Wang B, Tian X, Zhang Y, Li Y, Yang W, Zhang B, Wang W, Yang J, Li X (2018) Seismic signature of an untuned large-volume airgun array fired in a water reservoir. Seismol Res Lett 89(3):983–991. https://doi.org/10.1785/0220180007

Xu Y, Su YJ, Qin JZ (2004) Development of Q-value studies. J Seismol Res 27(4):385–389. https://doi.org/10.3969/j.issn.1000-0666.2004.04.019

Yamaoka K, Miyamachi H, Watanabe T, Kunitomo T, Michishita T, Ikuta R, Iguchi M (2014) Active monitoring at an active volcano: amplitude-distance dependence of ACROSS at Sakurajima Volcano, Japan. Earth Planets Space 66(1):32. https://doi.org/10.1186/1880-5981-66-32

Yang W, Wang B, Ge H, Wang W, Chen Y (2013) The active monitoring system with large volume airgun source and experiment. Earthq Res China 29(4):399–410. https://doi.org/10.3969/j.issn.1001-4683.2013.04.001

Yang H, Duan Y, Song J, Jiang X, Tian X, Yang W, Wang W, Yang J (2020) Fine structure of the Chenghai fault zone, Yunnan, China, constrained from teleseismic travel time and ambient noise tomography. J Geophys Res Solid Earth. https://doi.org/10.1029/2020JB019565

Yoshimoto K, Sato H, Ohtake M (1993) Frequency-dependent attenuation of P and S waves in the Kanto area, Japan, based on the coda-normalization method. Geophys J Int 114:165–174. https://doi.org/10.1111/j.1365-246X.1993.tb01476.x

Yoshimoto K, Sato H, Iio Y, Ito H, Ohminato T, Ohtake M (1998) Frequency-dependent attenuation of high-frequency P and S waves in the upper crust in western Nagano, Japan. Pure Appl Geophys 153:489–502. https://doi.org/10.1007/s000240050205

Zhang YP, Wang BS, Lin GQ, Wang WT, Yang W, Wu ZH (2020) Upper crustal velocity structure of Binchuan, Yunnan revealed by dense array local seismic tomography. Chin J Geophys 63(9):3292–3306. https://doi.org/10.6038/cjg2020N0455

Zhou L, Zhao C, Xiu J, Chen Z, Zheng S (2008) Methods and developments of research on crustal Q value by using earthquakes. Recent Dev World Seismol 350:1–11. https://doi.org/10.3969/j.issn.0253-4975.2008.02.001

Publisher's Note